Earth Planets Space, **60**, 365–373, 2008

Equivalent source mapping of the lunar crustal magnetic field using *ABIC*

M. Toyoshima[1], H. Shibuya[1], M. Matsushima[2], H. Shimizu[3], and H. Tsunakawa[2]

[1]*Department of Earth Sciences, Kumamoto University, Kumamoto, Japan*
[2]*Department of Earth and Planetary Sciences, Tokyo Institute of Technology, Tokyo, Japan*
[3]*Earthquake Research Institute, University of Tokyo, Tokyo, Japan*

(Received March 1, 2007; Revised October 10, 2007; Accepted November 10, 2007; Online published April 9, 2008)

An objective scheme is presented for estimating the lunar crustal magnetic field from the LMAG (Lunar MAGnetometer) data of the SELENE ("KAGUYA") spacecraft. Our scheme improves the equivalent source method in three respects. The first improvement is that the source calculation is performed simultaneously with detrending. The second is that a great number of magnetic charges (magnetic monopoles) are used as the equivalent sources. The third is that the distribution of the magnetic charges is detremined by the damped least squares method, and the optimum smoothness is determined objectively by minimizing Akaike's Bayesian Information Criterion (*ABIC*). For testing the scheme, we apply it to the Lunar Prospector magnetometer data in the region centered at the Reiner Gamma magnetic anomaly. The magnetic field map at an altitude of 20 km is stably drawn from datasets for different altitudes (18 km and 34 km). The *ABIC* minimizing criterion successfully controls the smoothness due to the numerical damping and extracts as much information as possible from the given data. This scheme will help produce a coherent lunar magnetic anomaly map by integrating the observations from various altitudes of the SELENE and previous missions.

Key words: Equivalent source, *ABIC*, lunar crustal magnetic field, Reiner Gamma.

1. Introduction

JAXA (Japan Aerospace Exploration Agency) has launched a lunar-orbiting satellite, SELENE ("KAGUYA") on September 14, 2007 from the Tanegashima Space Center. It was placed into a peripolar orbit at an altitude of about 100 km. Among many scientific instruments, it has a 3-component magnetometer (LMAG: Lunar MAGnetometer) primarily for mapping the crustal magnetic field of the Moon. Observations will continue for 1 year, and the LMAG investigator team is requesting optional observations at lower than 50 km altitude after the nominal mission.

The LMAG is composed of a set of orthogonal three fluxgate sensors attached on the tip of a 12 m mast, a pair of coils for determining the alignment of the satellite and the sensors (Shimizu *et al*., 2008), and an electronics control box. The noise level of the sensor is less than 0.1 nT, and the interval of measurement is 1/32 sec. We expect that the SELENE LMAG data will fill the gaps of the Lunar Prospector's (LP) magnetometer data.

For the first scientific results, we are planning to complete the lunar crustal magnetic anomaly map, combining the SELENE magnetometer data and those of previous satellites. Several methods have been used for mapping the lunar crustal magnetic field from the orbital measurements. One of the major difficulties in processing the satellite magnetometer data, aside from the influence of the external magnetic field, is the variation in the altitude of the measurements. In lunar crustal field mapping, approximately constant altitude maps have often been provided by a two-dimensional averaging (Hood *et al*., 1979, 1981, 2001; Richmond *et al*., 2003). In this method, the fluctuation of the magnetic field is smoothed by using a moving boxcar method. Richmond *et al*. (2005) and Richmond and Hood (2007) calculated the upward continuation of low altitude data to higher constant altitude by assuming an empirical power law dependence estimated by fitting to observations at several altitudes. Kurata *et al*. (2005) estimated the magnetic field by solving a nonlinear inverse-problem. They modeled the magnetic anomaly sources as magnetic dipoles buried beneath the lunar surface, and determined their directions, magnetic moments, and positions.

The SELENE extended mission may possibly have different altitudes than the LP spacecraft, so that mapping by two-dimensional averaging with empirical altitude compensation would be difficult to implement when combining both data for better resolution. We therefore develop an alternate objective scheme for estimating the spatial distribution of crustal magnetic field from observations data at different altitudes. In our scheme, the magnetic field is estimated by solving a linear inverse-problem that determines the sources distributed on the lunar surface which satisfy the observational data. This is known as the equivalent source method (e.g. Dyment and Arkani-Hamed, 1998). Our scheme improves this method in three features. The first feature is that the source calculation is performed simultaneously with detrending. The second is that magnetic charges (magnetic monopoles) are used as the equivalent sources. Although there are no magnetic monopoles in nature, it is mathematically convenient to make use of them, as explained in Section 2 below. The third is that the number

of sources is large enough to get a smooth magnetic field at the observation height. It can be larger than the number of measurements and the distribution of the magnetic charges is estimated by the damped least squares. The optimum smoothness is determined objectively by minimizing Akaike's Bayesian Information Criterion (*ABIC*). For testing the scheme, we apply it to the Lunar Prospector (LP) magnetometer data, and provide the magnetic field map in the region centered at the Reiner Gamma magnetic anomaly, one of the strongest anomaly groups on the Moon (Hood *et al.*, 2001). Since this region is the most intensively studied and has been previously mapped (Hood *et al.*, 1979, 1981, 2001; Kurata *et al.*, 2005), it is one of the best areas for comparing different methods.

2. Method

We take the approach of the equivalent source method for estimating the 3-d magnetic field. This entails solving a linear inverse-problem to determine the magnetic sources distributed on the surface of the Moon (with the radius of 1738 km) that satisfy the observational data. The method has been used for mapping the crustal magnetic fields of Mars and Earth (e.g., Purucker *et al.*, 2000; Langlais *et al.*, 2004; Chiao *et al.*, 2006; Nicolosi *et al.*, 2006). Recently, the method has also been applied in an attempt to map a part of the lunar farside (Purucker *et al.*, 2006) and the lunar south pole region (Schaler and Purucker, 2007). The equivalent source technique represents the observational magnetic field $\hat{B}_i$ at an observational point i as

$$\hat{B}_i = \sum_j (\hat{\omega}_{ij} J_j) + \hat{\varepsilon}_i \tag{1}$$

where J_j is the intensity of the j-th source at or below the surface of the Moon, $\hat{\varepsilon}_i$ is the residual vector (including the observational error) at the i-th point, and $\hat{\omega}_{ij}$ is the kernel function (Nicolosi *et al.*, 2006) giving the magnetic field at i-th point produced by j-th source of unit intensity.

Magnetic dipoles are widely used as the sources. However, the sources can be any shape, so long as they produce a divergent free potential field above the surface. We use magnetic charges (magnetic monopoles) rather than dipoles as the equivalent sources, for ease of calculation and smoothness of field generated by a source. Of course, we do not consider that the real sources of the lunar magnetic field are monopoles, but since the determination of the real sources of the potential field is not possible without another postulate, monopoles are as valid as dipoles as virtual sources. The kernel $\hat{\omega}_{ij}$ for a monopole source is given by

$$\hat{\omega}_{ij} = \frac{\hat{r}_{ij}}{4\pi r_{ij}^3} \tag{2}$$

where $\hat{r}_{ij}$ is the vector from the j-th magnetic charge to the i-th observational point. The charges are set on a fine grid with a larger number of charges than observations to avoid any influence of the grid phase on the result. Their intervals are small enough to avoid irregularities in the magnetic field.

In addition, the source calculation is performed simultaneously with detrending (removing the time varying interplanetary field). The trend has been reduced by subtracting a quadratic polynomial fitted to each component of the orbital data (Hood *et al.*, 1979). It is usually applied in the long segment of orbits. If the reduction is calculated in a short segment, the calculated trend includes the crustal field itself, and the reduction tends to over-detrend. In the present method (simultaneous detrending), coefficients of the polynomial and equivalent sources are determined simultaneously, adding the detrending equations to the equivalent source equations. The trend and the crustal magnetic field are distinguished by using some observational datasets at different altitudes, since a series of charges producing a polynomial trend at one altitude does not produce a field described by another polynomial at a different altitude. This makes it possible to use higher order polynomials for the trend function and/or a shorter segment of the orbit. We use here cubic polynomials for reducing the trend. If the number of observation points is M, and the total number of charges is N, then $\hat{B}_i$ is represented as

$$\hat{B}_i = \sum_{j=1}^{N} (\hat{\omega}_{ij} J_j) + (\hat{a}_k x_i^3 + \hat{b}_k x_i^2 + \hat{c}_k x_i + \hat{d}_k) + \hat{\varepsilon}_i \qquad (i = 1, 2, \cdots, M, \quad k = 1, 2, \cdots, S) \tag{3}$$

where x_i is the latitude at an observational point, k represents an orbital segment, and S is the number of orbital data segments. Rewriting Eq. (3) in matrix notation gives

$$B = \begin{pmatrix} \omega & X \end{pmatrix} \begin{pmatrix} J \\ A \end{pmatrix} + \varepsilon \tag{4}$$

where A is the coefficient matrix of the cubic polynomial.

The calculation of the magnetic charges and the cubic polynomial coefficients is usually performed by linear least squares. However, the total number of charges N in this case is more than the number of observation points M, and as a result J is undetermined. Since N always exceeds M, we introduce a damping constraint that the juxtaposed charges are not much different. Consequently, Eq. (4) becomes

$$\begin{pmatrix} B \\ 0 \end{pmatrix} = \begin{pmatrix} \omega & X \\ \alpha D & 0 \end{pmatrix} \begin{pmatrix} J \\ A \end{pmatrix} + \varepsilon \tag{5}$$

and the estimation of the matrix J and A can be achieved by solving the damped least squares. Assuming the lunar crustal magnetic field around the anomaly region is 0 nT (it can be postulated for the Moon by taking an appropriate region), the damping matrix D is defined as

$$D = \begin{pmatrix} -4 & 1 & & & 1 & & 0 \\ 1 & \ddots & \ddots & & & \ddots & \\ & \ddots & \ddots & \ddots & 0 & & 1 \\ & & \ddots & \ddots & \ddots & & \\ 1 & & 0 & \ddots & \ddots & \ddots & \\ & \ddots & & & \ddots & \ddots & 1 \\ 0 & & 1 & & & 1 & -4 \end{pmatrix}. \tag{6}$$

α denotes the hyper-parameter representing the strength of damping. In the equivalent source method, it is always

Table 1. Two LP magnetometer datasets used for testing the scheme at the Reiner Gamma anomaly. Model L uses two low altitude (∼18 km) datasets and one high altitude (∼100 km) one. Model M uses two middle altitudes (∼35 km) and a high altitude one.

Date	Altitude [km]	Observational points	Data segments
<Model L: low altitude group>			
February 23–24, 1999	17.6–19.2	461	9
March 22–23, 1999	17.1–18.9	486	10
April 28–29, 1998 (*)	90.6–93.2	542	10
Total		1489	29
<Model M: middle altitude group>			
May 16, 1999	32.8–35.2	447	9
June 12–13, 1999	32.6–34.9	483	10
April 28–29, 1998 (*)	90.6–93.2	542	10
Total		1472	29

(*Same dataset)

a problem to determine the damping hyper-parameter α. Akaike (1980) gave a criterion based on the assumption that both the residuals and the 2nd differentials of the sources have normal distributions. The damping hyper-parameter α is interpreted as the ratio of the dispersions of the distributions. The optimum value of α can be determined objectively by minimizing Akaike's Bayesian Information Criterion (*ABIC*). The *ABIC* is calculated in the same way as given by Oda and Shibuya (1996).

$$\begin{aligned} ABIC =& M \log \beta - N \log \alpha^2 - \log |D^t D| \\ &+ \log \left| \left(\omega \; X\right)^t \left(\omega \; X\right) + \alpha^2 D^t D \right| \\ &+ M - M \log M + M \log 2\pi + 2, \\ \beta =& \min \left\{ \left|\left| B - \left(\omega \; X\right) \begin{pmatrix} J \\ A \end{pmatrix} \right|\right|^2 + \alpha^2 \, ||DJ||^2 \right\}. \end{aligned} \tag{7}$$

The calculation of α that gives the minimum *ABIC* is not analytical, but, since it behaves well, it is easy to obtain by trial and error.

If this scheme works, the total charge, the sum of the charges, should be zero since there is no magnetic monopole in the universe. It provides a measure of how well the model works. With ill-shaped data, the total charge may be larger than the error. In such a case, one can easily add another constraint that the total charge is zero, adding a line in Eq. (5).

3. Application to the Reiner Gamma Magnetic Anomaly

In order to test the scheme, we apply it to the LP magnetometer data, and provide magnetic field maps in the region centered at the Reiner Gamma anomaly. This anomaly is located in western Oceanus Procellarum on the lunar nearside and is one of the strongest anomaly groups on the Moon (Hood *et al.*, 2001). The range of the mapping region is from 53° to 63°W longitude, and from 1° to 15°N latitude. We took the LP magnetometer data from the Planetary Plasma Interactions (PPI) node of the NASA's Planetary Data System (PDS). For crustal magnetic field studies, it is important to select the dataset in a quiet magnetic environment, such as the lunar wake or the geomagnetic tail lobe (Hood *et al.*, 2001). Even in the relatively quiet environments, there could be noisy duration due to some interplanetary field etc., thus visual inspection selecting the dataset to use is important. Since the LP changes its path in

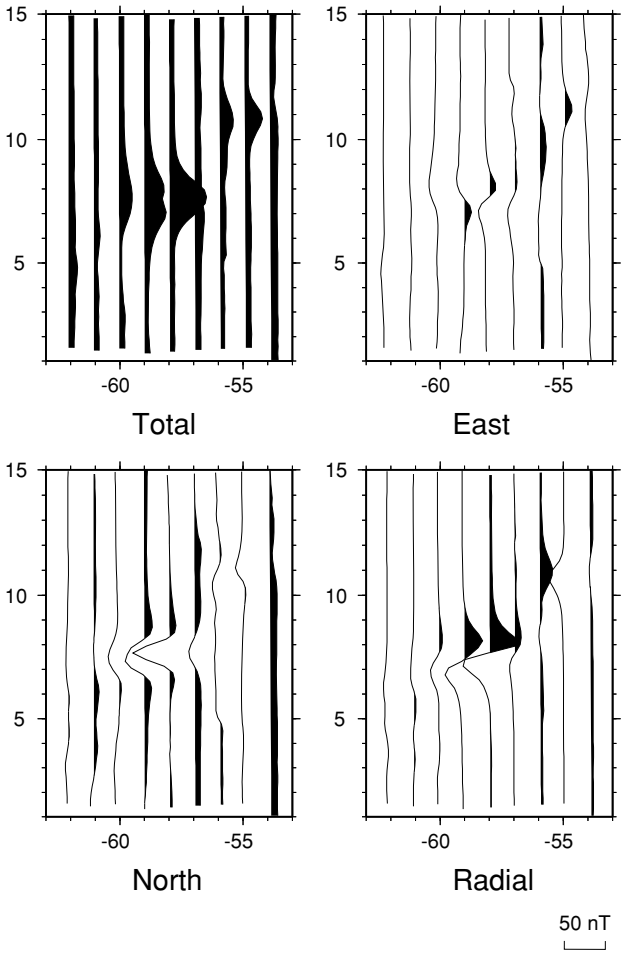

Fig. 1. Observational magnetic field components and total intensity along the orbital paths in the Reiner Gamma region during February 23–24 of 1999. The positive area is shaded in black.

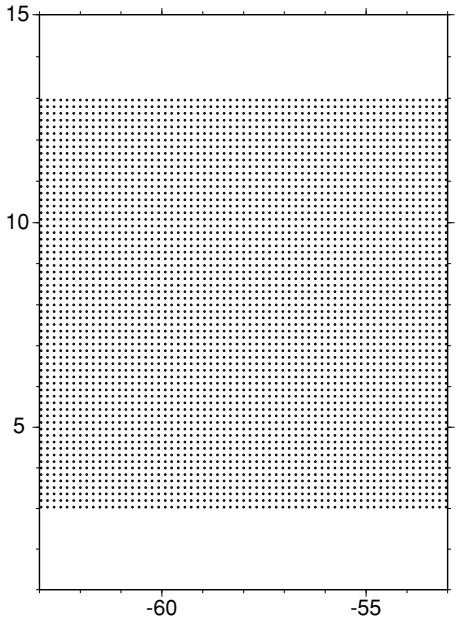

Fig. 2. Arrangement of magnetic charges in the mapping region. The magnetic charges are set on the lunar surface. The grid interval is as fine as 0.16°, and the number of charges N is 3969.

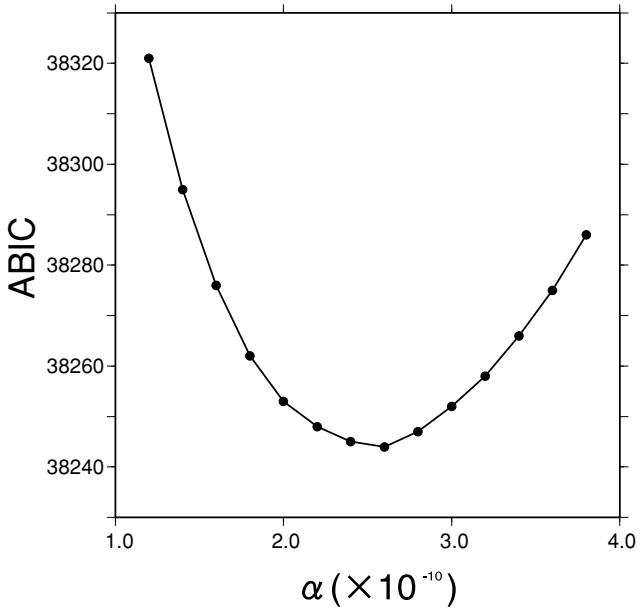

Fig. 3. *ABIC* values plotted versus the hyper-parameter α for the middle altitude data group. The step for searching for the optimum α is 2.0×10^{-11}. *ABIC* goes to a minimum value of 38244 where α equals to 2.6×10^{-10}.

longitude by one degree every two hours, a series of coherent altitude paths covering the analyzed region is produced. We call the data taken by the series as a dataset. At the Reiner Gamma region, there are 19 datasets taken during quiet times. They are divided into low (∼18 km), middle (∼35 km) and high (∼100 km) altitude datasets. One of the three low altitude datasets is incomplete in coverage, so that the datasets of average altitudes of 18.0 km and 18.4 km are used in this study. One dataset at a middle altitude is also incomplete in coverage, and we used two remaining datasets, whose average altitudes are 33.8 km and 34.0 km. Another dataset at 91.9 km altitude is used to stabilize the detrending. Table 1 summarizes the paths, and Fig. 1 shows the February 23–24, 1999 dataset, as an example.

In order to see how the scheme works with datasets of different altitude, we made two magnetic anomaly maps using each of two groups of datasets: One is with two low altitude (∼18 km) datasets and one high altitude (∼100 km) one (model L). The other is with two middle altitudes (∼35 km) and a high altitude one (model M).

As described above, the magnetic charges are arranged on a fine grid on the lunar surface in a slightly smaller area of the observational points to avoid edge effect oscillations (Fig. 2). The grid interval is 0.16° (corresponding to about 4.8 km near the lunar equator), and the number of charges N is 3969. The equation is solved by using the generalized QR decomposition in the LAPACK routine, DGELS (Anderson *et al.*, 1995). The calculation is not difficult, and took about 10 min for each α. We calculated *ABIC* at different values of α in steps of 2.0×10^{-11} to search for the optimum value. The step is fine enough so that the difference of the resultant magnetic field between the juxtaposed steps is well below the error of the measurement (expected to be about 1 nT). The *ABIC* values reach minima when the α's are 1.2×10^{-10} and 2.6×10^{-10}, and the rms (root mean square) residual is 0.74 and 0.37 nT for model L and M, respectively (Fig. 3).

The anomaly map at 20 km in altitude is drawn from the two models (Fig. 4(a) and (b)). From a visual inspection, the morphologies of the estimated crustal magnetic fields are found to be very similar to each other, indicating that the scheme works very stably in both models. Figure 5 is a plot of the total force across the largest peak from south to north. The broader and lower (∼31 nT) peak of model M compared to model L (with a peak value of 38 nT) occurs because the former is equivalent to the latter with a smoothing filter. It corresponds to larger α, and indicates that the data from higher altitude have less information than data from a lower altitude. The *ABIC* minimization criterion successfully controls the smoothness of the models and extracts as much information as possible from the given data.

A mapping using high altitude (∼100 km) datasets (model H) is also attempted. Out of 13 high altitude datasets, we select six for the calculation (Table 2). The detrending with a cubic polynomial clearly results in overdetrending in this case, thus a quadratic polynomial is used. The resultant map at 20 km altitude is shown in Fig. 6. As seen in the figure, the estimated magnetic field is stable but much smoother than the other models, corresponding to the larger α (6.0×10^{-10}), which is automatically determined with *ABIC*. Although the dataset selection for model H is very dependent on the knowledge of models M and L, the result shows the possibility of utilizing high altitude datasets, if we can prepare objective criteria.

4. Discussion

We use magnetic monopoles as the equivalent sources instead of commonly used dipoles to obtain a smoother kernel function, i.e., a smoother magnetic field in the calculation space. It is pretty easy to translate the monopole result to

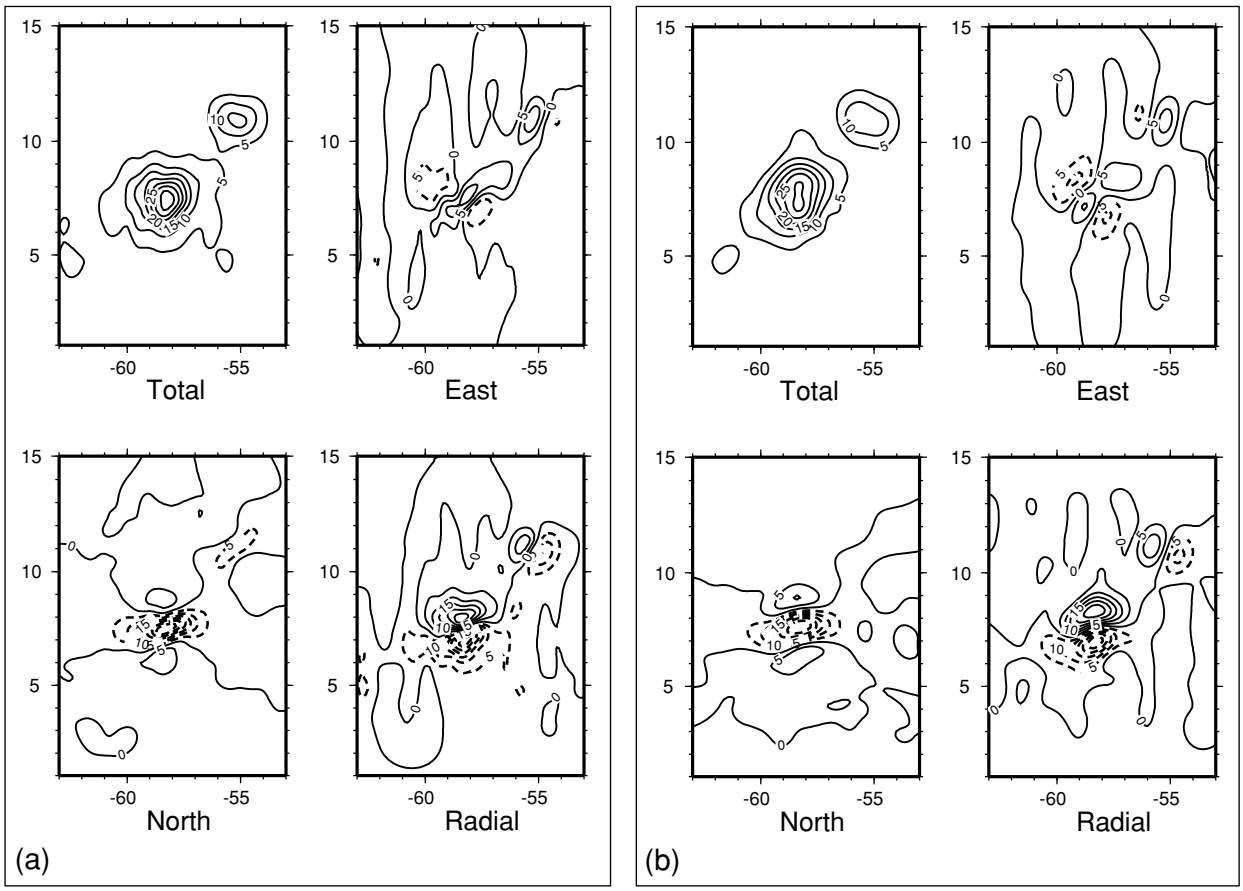

Fig. 4. Magnetic field maps computed from (a) model L and (b) model M at an altitude of 20 km. The contour interval is 5 nT. Dashed lines denote negative values.

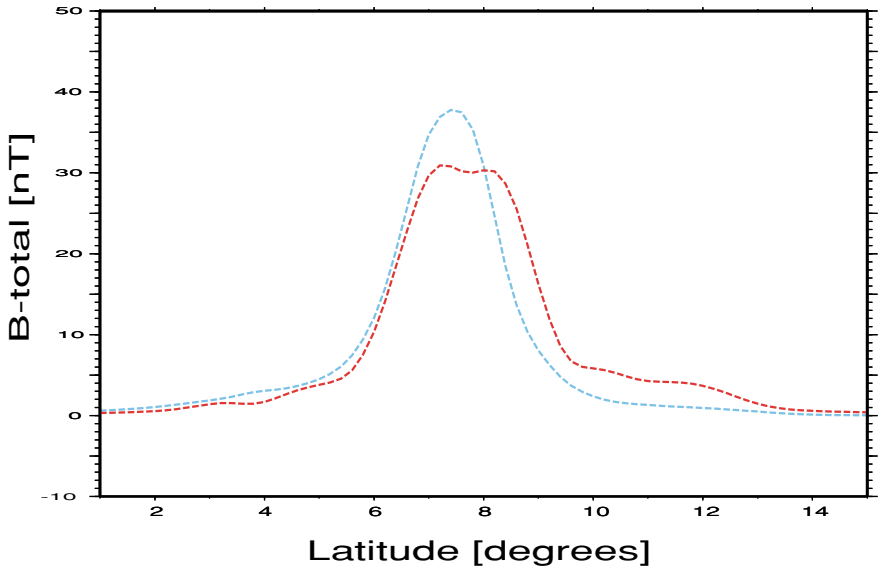

Fig. 5. Plot of the total field intensity across the largest peak from south to north. The dashed blue line and the dashed red line are the model fields calculated from models L and M, respectively.

the dipole distribution. Although the source dipoles can be oriented in any direction, it is seldom oriented in other than the x, y, and z directions. In the case of horizontal equivalent dipoles, the intensity of each dipole is readily calculated by taking difference of the sums of monopoles on both side of a grid point divided by the grid distance. The z-directed dipoles are also easily calculated considering that a magnetic field produced by a monopole J is equivalent to a distribution of dipoles on the x-y surface whose density ρ_d is given as $\rho_d = \frac{J}{2\pi\mu_0 R}$, where R is the distance from the monopole. For comparison to the grid distribution, the equivalent z-dipole sources at a grid point j are given as

Table 2. Six high altitude datasets used for estimating the magnetic field at an altitude of 20 km (model H).

Date	Altitude [km]	Observational points	Data segments
April 1–2, 1998	103.6–106.0	530	10
April 28–29, 1998	90.6–93.2	542	10
May 12–13, 1998	89.4–93.0	490	9
May 26, 1998	103.0–104.9	458	9
June 8–9, 1998	102.9–106.0	491	9
December 3–4, 1998	91.7–93.1	475	9
Total		2986	56

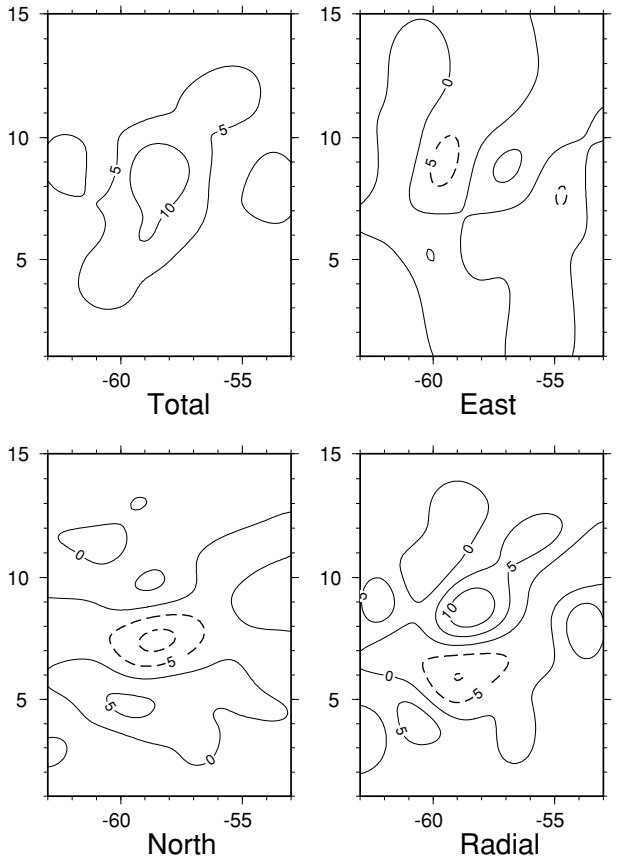

Fig. 6. Magnetic field maps computed from model H at an altitude of 20 km. The contour interval is 5 nT. Dashed lines denote negative values.

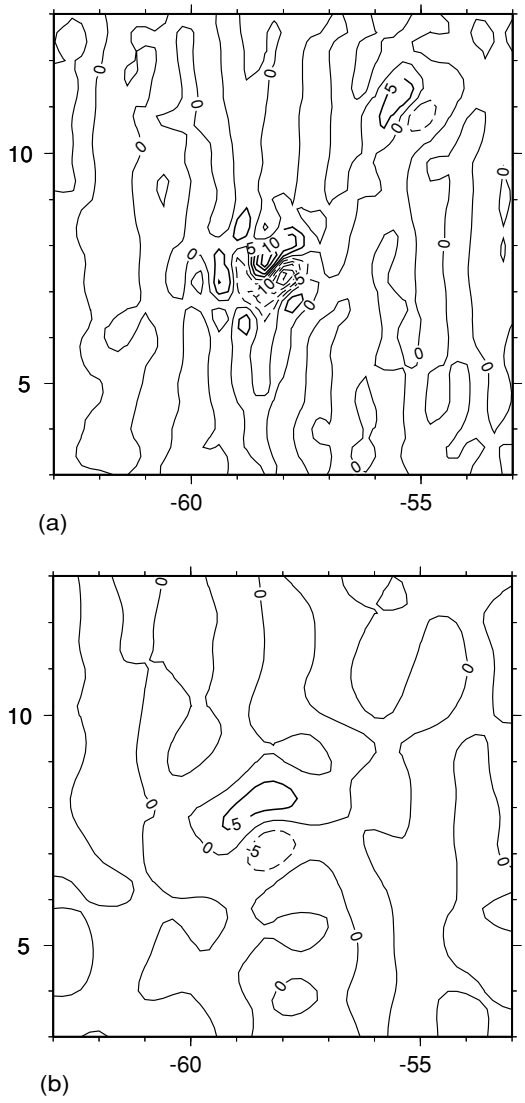

Fig. 7. Contour map of magnetic charges calculated with optimum α in (a) model L and (b) model M. The contour interval is 5 Wb. Dashed lines denote negative values.

$\frac{d^2}{2\pi\mu_0}\sum\frac{J_i}{R_{ij}}$, where d is the grid distance and R_{ij} is the distance between the i-th monopole source and j-th z-dipole source. Therefore, calculation with virtual monopoles has no disadvantage compared to using dipoles for estimating the real magnetic sources. Instead, easy translation may help the interpretation of the map.

Figure 7(a) and (b) shows the magnetic charge distribution for optimum α for models L and M, respectively. The total charge is -131 Wb (corresponding to about 1.5% of the mean of the absolute values) for model L and -135 Wb (corresponding to about 2.6% of the mean of the absolute values) for model M. The magnetic field created by the total charge is far smaller than the error at the satellite altitude. It also shows the validity of the model.

The problem of total charge is closely related to the detrending of each path. If the detrending is inappropriate, there remains a bias in the magnetic field, which results in significantly non-zero charge in our model. A small total charge indicates the validity of the detrending calculation. As the matter of fact, it is easily seen in Fig. 8(a) that the detrending polynomial does not have swell around the

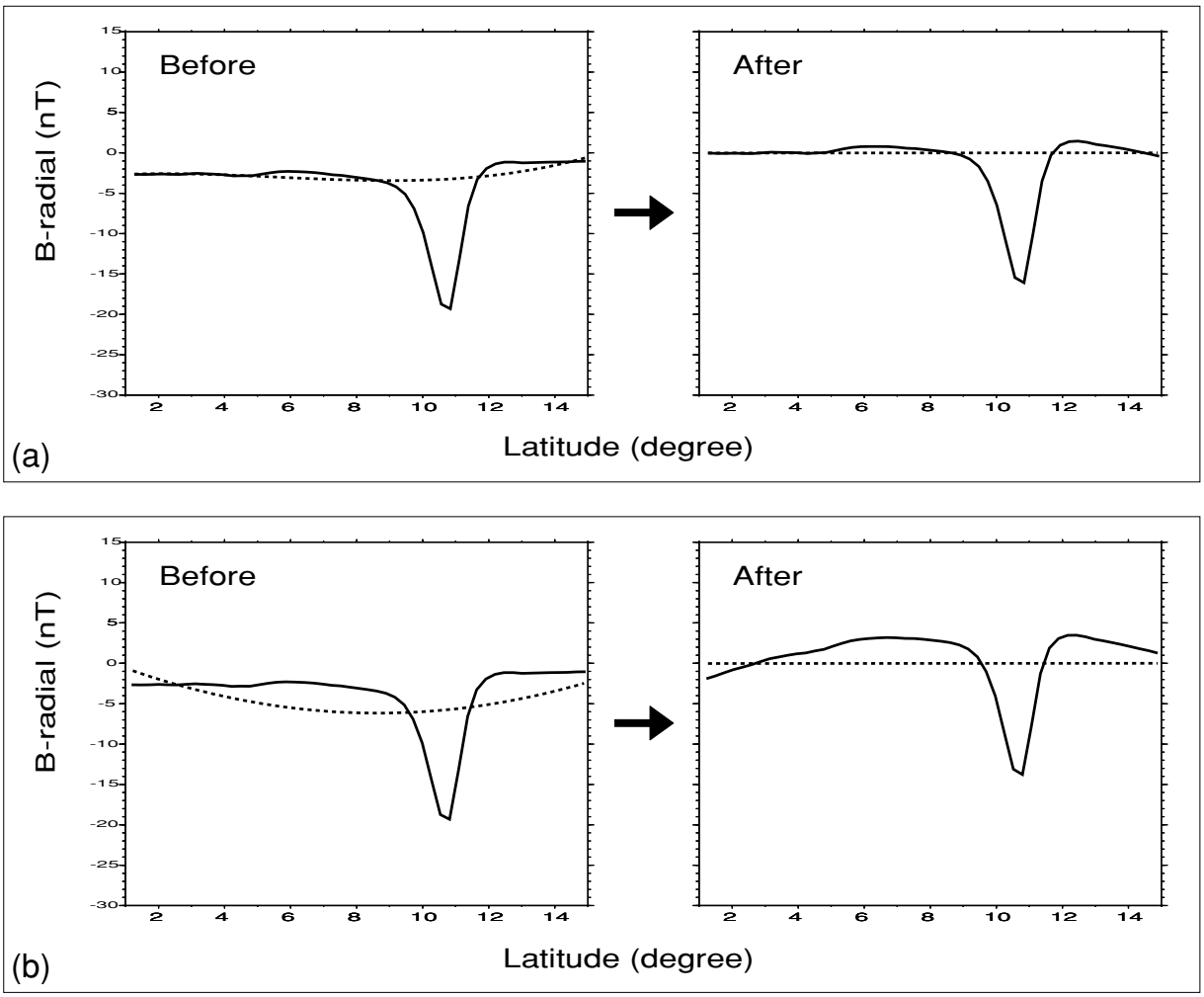

Fig. 8. Comparison of the detrending methods, (a) the simultaneous and (b) direct methods. The path shown is from the low altitude dataset (obtained during February 23–24 of 1999) at about 55°W longitude, which is shown in Fig. 1.

crustal field source. On the other hand, the direct detrending (Fig. 8(b)) tends to have the problem of over-detrending. The detrending procedure has been employed on longer paths to avoid over-detrending (Hood *et al*., 2001). Using the present method, we can correct for the contribution of the planetary field to shorter wavelength.

The models are also compared with one of the observational datasets at low altitude. Figure 9 shows the observed total forces on the tracks 56.9°, 57.9° and 59.0°W in longitude, on February 23–24, 1999, along with calculated ones from models L and M. Model L naturally fits the data, since the model is prepared with the data themselves. Model M suffers from some smoothing due to the larger α, which can be clearly seen on the 57.9°W path, but reproduces the observations fairly well.

For comparison to the Reiner Gamma anomaly map by two-dimensional filtering (Hood *et al*., 2001), we construct a total force map at the altitudes of 18 km from model M (Fig. 10(a)). The averaging flattens the peak to 20 nT (Fig. 10(b)), which is much smaller than the observed maximum of about 45 nT (after detrending). On the other hand, the maximum in Fig. 10(a) is about 37 nT. In spite of the use of higher altitude data, the present method expresses more detail of the crustal field than the Hood *et al*. (2001) estimation.

Kurata *et al*. (2005) also give similar results. In the Reiner Gamma region, the crustal field is pretty simple and represented by a couple of dipoles. This fact allows their method to achieve good fitting with two dipoles in the Reiner Gamma anomaly. As the number of parameters is greatly different, our fitting gives a better residual, so that, for the 3-d magnetic field estimation, the equivalent source method has a clear advantage. On the other hand, the dipole representation by Kurata *et al*. (2005) has the benefit of focusing on the real source of the anomaly. The method can be used for mapping of the crustal field using many dipoles. In that case, the non-linear nature of their method results in a large disadvantage in calculation time and robustness. The advantage of a linear inversion, on which the present method is based, is that minimizing parameters are analytically found so that calculation is easy and does not depend on the initial state.

The objectivity of this method also derives from the linearity. It does not need an initial seed for the calculation. The only parameter we have to vary is the damping parameter α in the inversion. It is then determined by minimizing *ABIC*. It means that the data themselves determine the damping parameter. Thus, there is no adjustable parameter

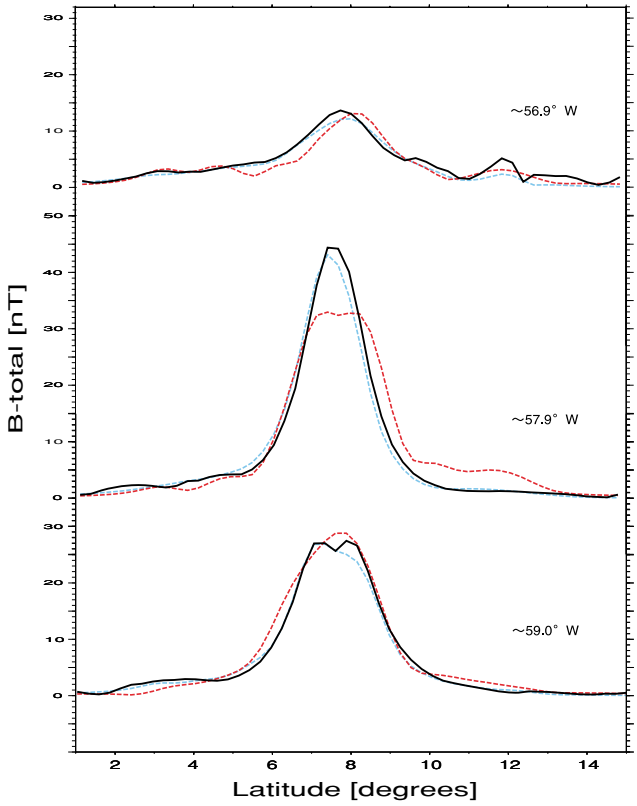

Fig. 9. Three total field intensity plots along the orbital paths around the largest peak. The black line is based on the detrended observational field on February 23–24 of 1999. The dashed blue line and dashed red line are the model fields calculated from models L and M, respectively. Each model field is estimated at the observational altitude.

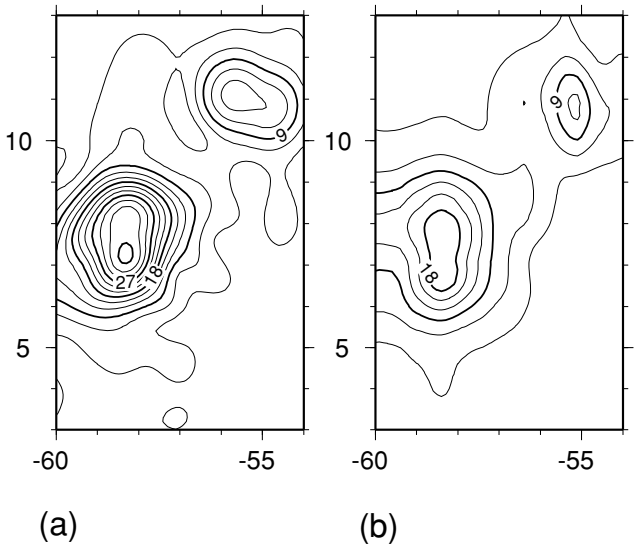

Fig. 10. (a) Contour map of the total magnetic field intensity computed by our method (using model M) and (b) two-dimensional filtered map (Hood *et al.*, 2001), at an altitude of 18 km. In the two maps, the contour interval is 3 nT.

in the calculation. It guarantees the objectivity of the whole scheme and the independence of the results from the calculation process. The objectivity and ease of calculation in this scheme makes it possible to process the massive data that will be supplied by the SELENE mission.

5. Conclusion

In this study, we develop a new scheme for the 3-d estimation of the lunar crustal magnetic field from orbital measurements. This scheme improves the equivalent source method in the following three ways.

(1) A large number of magnetic charges (magnetic monopoles) are used as the sources.
(2) The detrending is performed simultaneously with the source calculation, using cubic polynomials.
(3) The estimation of the magnetic charges is solved by damped least squares, and the optimum smoothness is determined by minimizing *ABIC*.

As a result of application to the Reiner Gamma anomaly, the magnetic filed was stably estimated at altitudes of 20 km from models L and M. This stable estimation from two models shows that the *ABIC* minimizing criterion successfully controls the smoothness and extracts as much information about the crustal field as possible from the given data. This scheme is completely objective and does not need massive computing power. As the scheme can coherently handle the data from different altitudes, it is easy to integrate the SELENE LMAG data with those of previous missions, and we expect the coverage of the magnetic anomaly map will improve significantly after the SELENE mission.

Acknowledgments. We are grateful to Benoit Langlais and an anonymous reviewer for their helpful comments. We also thank G. Schubert for improving the manuscript.

References

Akaike, H., Likelihood and the Bayes procedure, in *Bayesian Statistics*, edited by J. M. Bernard, M. H. Degroot, D. V. Lindley, and A. F. M. Smith, pp. 143–166, Univ. Valencia, Spain, 1980.

Anderson, E., Z. Bai, C. Bischof, J. Demmel, J. Dongarra, J. Du Croz, A. Greenbaum, S. Hammarling, A. McKenney, S. Ostrouchov, and D. Sorensen, *LAPACK User's Guide Second Edition*, 260 pp., Society for Industrial and Applied Mathematics, Philadelphia, 1995.

Chiao, L. Y., J. R. Lin, and Y. C. Gung, Crustal magnetization equivalent source model of Mars constructed from a hierarchical multiresolution inversion of the Mars Global Surveyor data, *J. Geophys. Res.*, **111**, E12010, doi:10.1029/2006JE002725, 2006.

Dyment, J. and J. Arkani-Hamed, Equivalent Source Magnetic Dipoles Revisited, *Geophys. Res. Lett.*, **25**, 2003–2006, 1998.

Hood, L. L., P. J. Coleman Jr., and D. E. Wilhelms, Lunar nearside magnetic anomalies, *Proc. Lunar Planet. Sci. Conf., 10th*, 2235–2257, 1979.

Hood, L. L., C. T. Russell, and P. J. Coleman Jr., Contour maps of lunar remanent magnetic fields, *J. Geophys. Res.*, **86**, 1055–1069, 1981.

Hood, L. L., A. Zakharian, J. Halekas, D. L. Mitchell, R. P. Lin, M. H. Acuna, and A. B. Binder, Initial mapping and interpretation of lunar crustal magnetic anomalies using Lunar Prospector magnetometer data, *J. Geophys. Res.*, **106**, 27825–27839, 2001.

Kurata, M., H. Tsunakawa, Y. Saito, H. Shibuya, M. Matsushima, and H. Shimizu, Mini-magnetosphere over the Reiner Gamma magnetic anomaly region on the Moon, *Geophys. Res. Lett.*, **32**, L24205, doi:10.1029/2005GL0244097, 2005.

Langlais, B., M. Purucker, and M. Mandea, Crustal magnetic field of Mars, *J. Geophys. Res.-Planets*, **109**, E02008, doi:10.1029/2003JE002048, 2004.

Nicolosi, I., I. Blanco-Montenegro, A. Pignatelli, and M. Chiappini, Estimating the magnetization direction of crustal structures by means of an equivalent source algorithm, *Phys. Earth Planet. Inter.*, **155**, 163–169, 2006.

Oda, H. and H. Shibuya, Deconvolution of long-core paleomagnetic data of Ocean Drilling Program by Akaike's Bayesian Information Criterion minimization, *J. Geophys. Res.*, **101**, 2815–2834, 1996.

Purucker, M., D. Ravat, H. Frey, C. Voorhies, T. Sabaka, and M. Acuna, An altitude-normalized magnetic map of Mars and its interpretation,

Geophys. Res. Lett., **27**, 2449–2452, 2000.

Purucker, M., T. Sabaka, N. Tsyganenko, N. Olsen, J. Halekas, and M. Acuna, The Lunar magnetic field environment: Interpretation of new maps of the internal and external fields, *Lunar Planet. Sci., XXXVII*, abstract 1933, 2006.

Richmond, N. C. and L. L. Hood, A preliminary global map of the vector lunar crustal magnetic field based on Lunar Prospector magnetometer data, *J. Geophys. Res.*, 2007 (in press).

Richmond, N. C., L. L. Hood, J. S. Halekas, D. L. Mitchell, R. P. Lin, M. H. Acuna, and A. B. Binder, Correlation of a strong lunar magnetic anomaly with a high-albedo region of the Descartes mountains, *Geophys. Res. Lett.*, **30**, 1395, doi:10.1029/2003GL016938, 2003.

Richmond, N. C., L. L. Hood, D. L. Mitchell, R. P. Lin, M. H. Acuna, and A. B. Binder, Correlations between magnetic anomalies and surface geology antipodal to lunar impact basins, *J. Geophys. Res.*, **110**, E05011, doi:10.1029/2005JE002405, 2005.

Schaler, E. W. and M. E. Purucker, Lunar south pole hydrogen & water ice deposits: Constraints from Lunar Prospector magnetic field observations, *Lunar Planet. Sci., XXXVIII*, abstract 1034, 2007.

Shimizu, H., F. Takahashi, N. Horii, A. Matsuoka, M. Matsushima, H. Shibuya, and H. Tsunakawa, Ground calibration of the high-sensitivity SELENE lunar magnetometer LMAG, *Earth Planets Space*, **60**, this issue, 353–363, 2008.

M. Toyoshima (e-mail: m.toyo@es.sci.kumamoto-u.ac.jp), H. Shibuya, M. Matsushima, H. Shimizu, and H. Tsunakawa